Synchronization Stability Enhancement of Grid-Following Converter Under Inductive Power Grid

Hu, Bin; Zhao, Chen; Sahoo, Subham; Wu, Chao; Chen, Liang; Nian, Heng; Blaabjerg, Frede

Published in:
I E E E Transactions on Energy Conversion

DOI (link to publication from Publisher):
10.1109/TEC.2023.3265518

Publication date:
2023

Document Version
Accepted author manuscript, peer reviewed version

Citation for published version (APA):
Hu, B., Zhao, C., Sahoo, S., Wu, C., Chen, L., Nian, H., & Blaabjerg, F. (2023). Synchronization Stability Enhancement of Grid-Following Converter Under Inductive Power Grid. *I E E E Transactions on Energy Conversion*, *38*(2), 1485-1488. Article 10097528. https://doi.org/10.1109/TEC.2023.3265518

Synchronization Stability Enhancement of Grid-Following Converter under Inductive Power Grid

Bin Hu, *Student Member, IEEE*, Chen Zhao, Subham Sahoo, *Member, IEEE*, Chao Wu, *Member, IEEE*, Liang Chen, Heng Nian, *Senior Member, IEEE*, Frede Blaabjerg, *Fellow, IEEE*

***Abstract*—The loss of synchronization (LOS) is a main issue for dynamic behavior of grid-following converter (GFC) under inductive power grid. This letter reveals the underlying mechanism of insufficient damping or even negative damping during grid disturbance, and analyzes how the initial speed of angle-difference between PLL output and grid voltage affects the synchronization stability. Then a synchronization stability enhancement scheme to add a positive damping and a reverse angular frequency during transient process is proposed in this letter.**

***Index Terms*—Grid-following converter, phase-locked loop, inductive grid, synchronization stability.**

I. Introduction

With the rapid increase of renewable energy sources, the active and reactive power can be injected into the grid through the grid-following converter (GFC) [1]. Differing from the synchronous generator (SG), the synchronization dynamic behavior of GFC is highly affected by the phase-locked loop (PLL), which may cause the loss of synchronization (LOS) due to insufficient damping [2].

Some improved PLL structures during grid disturbance have been published previously, such as the frozen PLL [3], the adaptive parameter PLL [4] and the first-order PLL [5]. However, the frozen PLL lacks accurate phase angle detection [4]. The adaptive parameter PLL and the first-order PLL both focus on increasing the damping ratio. Nevertheless, modifying PLL parameters may cause some resonance issues [6]. The logic transitions and threshold values of first-order PLL are complicated to design [7]. And it is also worth analyzing other methods to further enhance the synchronization stability besides changing damping ratio.

This letter analyzes the underlying mechanism of insufficient damping or even negative damping for GFC under inductive power grid. In addition, this letter notices that the initial speed of angle-difference between PLL output and grid voltage is another important link to affect synchronization stability. To this end, an improved synchronization stability enhancement scheme related to the damping coefficient and initial angle speed is presented in this letter.

This work was supported by the National Natural Science Foundation of China under Grant 51977194. *(Corresponding author: Heng Nian.)*

B. Hu, C. Zhao and H. Nian are with the College of Electrical Engineering, Zhejiang University, Hangzhou, China (e-mail: 11810031@zju.edu.cn; eezhaochen@zju.edu.cn; nianheng@zju.edu.cn). S. Sahoo and F. Blaabjerg are with the Department of Energy, Aalborg University, Aalborg, Denmark. (email: sssa@energy.aau.dk; fbl@energy.aau.dk). C. Wu is with the Department of Electrical Engineering, Shanghai Jiao Tong University, Shanghai, China (e-mail: wuchao@sjtu.edu.cn). L. Chen is with the School of Information Science and Engineering, NingboTech University, Ningbo, China (e-mail: 21410077@zju.edu.cn).

II. LOS Mechanism for Grid-Following Converter under Inductive Power Grid

Fig. 1 illustrates the topology of GFC connected with weak grid. $\boldsymbol{U}_{pcc}$ and $\boldsymbol{I}_{pcc}$ represent the three-phase voltage and current at the point of common coupling (PCC). $\boldsymbol{U}_{gcp}$ represents the voltage at the grid connection point (GCP). $\boldsymbol{Z}_g=R_g+j\omega_g L_g$ is the grid impedance. L_f is the filter inductance. The dc-link voltage V_{dc} is assumed to be constant in this letter.

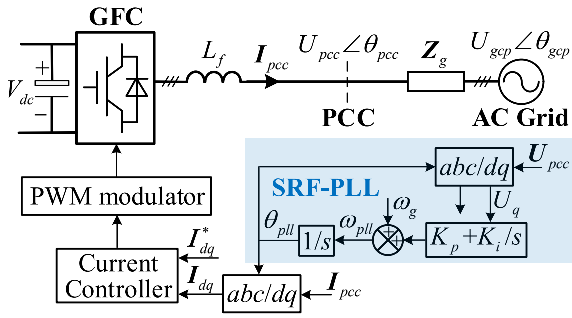

Fig. 1. Topology of grid-following converter connected with weak grid.

The GFC relies on the PLL to implement the grid synchronization, and the block diagram of the conventional synchronous reference frame PLL (SRF-PLL) is also depicted in Fig. 1, where the K_p and K_i are the proportional integral gains, ω_g=100π rad/s is the fundamental angular frequency. The dynamics of LOS lies in the low-frequency range [5], while the bandwidth of current controller is usually high, thus the synchronization stability of the GFC is dominated by the dynamics of the PLL. The PLL output angle θ_{pll} is equal to PCC voltage angle θ_{pcc} at the steady state, while $\theta_{pll}\neq\theta_{pcc}$ in the transient process. It can define the angle difference δ between PLL output and GCP voltage as shown in (1), and depict the voltage-angle curves as shown in Fig. 2, to characterize the phase-swing behavior of GFC. The steady-state and max-deviation of δ can be calculated in (2). Note that the LOS mechanism and synchronization stability enhancement under resistive dominated grid have been analyzed in [8]. For example, GFC may lose the synchronism under smaller grid voltage and larger grid resistance. This letter pays more attention on inductive dominated grid. When the grid impedance is pure inductive, i.e. R_g=0, the steady-state angle difference δ_0 is always positive.

$$\delta=\theta_{pll}-\theta_{gcp}=\int\left(K_p+K_i\int\right)\left(\omega_{pll}L_gI_d+R_gI_q-U_{gcp}\sin\delta\right) \tag{1}$$

$$\begin{cases} \delta_0 = \sin^{-1}\left(\dfrac{\omega_{pll}L_g I_d + R_g I_q}{U_{gcp}}\right) \\ \delta_{\max} = \pi - \sin^{-1}\left(\dfrac{\omega_{pll}L_g I_d + R_g I_q}{U_{gcp}}\right) \end{cases} \tag{2}$$

When the operating point of the converter-grid interconnected system changes, for example, changes from the point *a* to point *b*, the angle difference δ will move to a new steady state at δ_0, and the trajectory of δ can be seen as the purple solid curve in Fig. 2. Due to the inertial effect of integral loop, δ will continue to move. Due to the damping effect of proportional loop, δ will converge to δ_0 after several phase-swing periods [5]. However, when the angle overshoot exceeds the $\delta_{\max}$, the GFC will lose synchronization stability as shown in the purple dotted curve.

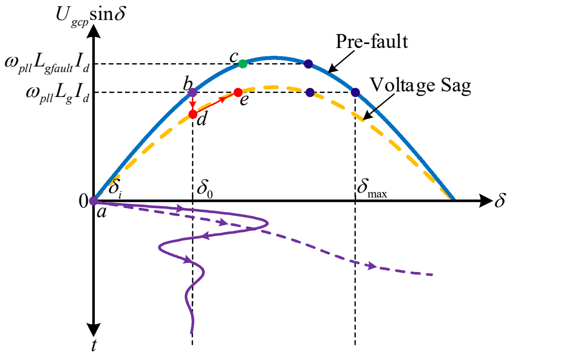

Fig. 2. Voltage-angle curves of grid-following converter under inductive grid.

It can be found that the GFC may occur LOS when the new steady-state angle difference δ_0 is larger than the initial one δ_i under weak inductive grid. There are three cases with increased angle difference:

- *Case 1:* GFC startups with increased active current, i.e. point *a* moves to point *b*.
- *Case 2:* Grid impedance increases to L_{gfault} during grid faults such as line tripping, i.e. point *b* moves to point *c*.
- *Case 3:* Grid voltage sags during grid faults such as short circuit, i.e. point *b* moves to point *d*, then moves to point *e*.

III. Effect of Damping and Initial Angle Speed on LOS

A. Compared with synchronous generator

The traditional swing equation of SG is as follow, where P_T is mechanical power, P_E is electromagnetic power, J and D are inertia and damping coefficient.

$$P_T - P_E = J\ddot{\delta} + D\dot{\delta} \tag{3}$$

The voltage-angle curve of GFC is similar to the power–angle curve of SG. However, the PLL-based system has two additional characteristics, i.e. maybe exist negative damping and the initial angle speed.

Fig. 3 depicts the phase portrait of (3) to clearly describe the influence of different damping coefficient D and initial angle speed δ_i', where the P_T=394.36 W, P_E=563.38sinδ W, δ_i=0, δ_0=0.78 rad, $\delta_{\max}$=2.36 rad, J=2.

According to Fig. 3 (a), it can be found that: 1) when there is no damping, i.e. D=0, the system is always in dynamic process; 2) when with the positive damping, i.e. D=10, the phase portrait will converge to steady state at δ_0; 3) when with the negative damping, i.e. D=-10, the system will lose synchronization; 4) when with a smaller negative damping, i.e. D=-1, the phase portrait is diverged, and finally occur LOS after several swing periods.

According to Fig. 3 (b), it can be found that: 1) when the initial angle speed increases, i.e. δ_i'=0.75, the phase portrait is closer to $\delta_{\max}$; 2) when the initial angle speed further increases, i.e. δ_i'=1.5, the phase portrait may exceed $\delta_{\max}$ and cause LOS; 3) when with the opposite initial angle speed, i.e. δ_i'=-1.5, the second half of trajectory is the same as δ_i'=1.5.

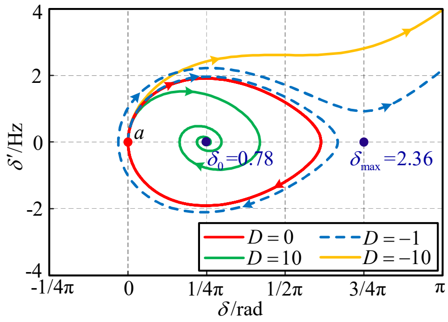

(a) initial angle speed is always zero but damping coefficient is different

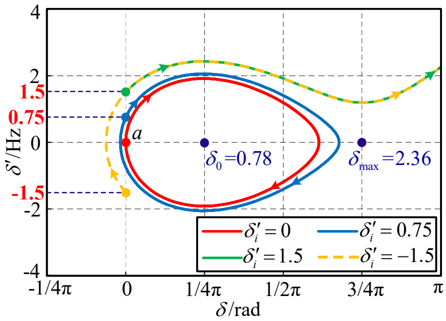

(b) damping coefficient is always zero but initial angle speed is different

Fig. 3. Phase portraits of swing equation.

Overall, it is desirable to have large positive damping and small absolute value of initial angle speed to enhance the synchronization stability.

B. Detailed transient model of grid-following converter

According to the detailed transient model of GFC, this section will analyze the causes and effects of negative damping and initial angle speed. Taking *Case 1* as an example, the GFC is controlled with the unity power factor, and the active current startups from 0 to the rated current $I_{\max}$.

- Assuming K_p=0, ω_{pll}=ω_g and performing differentiation of (1), the swing equation and initial angle speed are shown as,

$$\underbrace{\omega_g L_g I_{\max}}_{P_T} - \underbrace{U_{gcp}\sin\delta}_{P_E} = \underbrace{\frac{1}{K_i}}_{J}\delta'' \tag{4}$$

$$\delta_i' = 0 \tag{5}$$

It can be found that when considering K_i only, the initial angle speed is 0, and the GFC is similar to the SG without damping. If δ does not exceed $\delta_{\max}=\pi\text{-}\sin^{-1}(\omega_g L_g I_{\max}/U_{gcp})$ in the first swing period, the system will be stable.

- Considering K_p and K_i, assuming $\omega_{pll}=\omega_g$, the swing equation and initial angle speed are shown as,

$$\underbrace{\omega_g L_g I_{\max}}_{P_T} - \underbrace{U_{gcp}\sin\delta}_{P_E} = \underbrace{\frac{1}{K_i}}_{J}\delta'' + \underbrace{\frac{K_p U_{gcp}\cos\delta}{K_i}}_{D}\delta' \tag{6}$$

$$\delta_i' = K_p \omega_g L_g I_{\max} \tag{7}$$

It can be found that when considering K_p, the system has positive damping when δ is between 0 and 90°, while has negative damping when δ is between 90° and 180°. In addition, the system has the initial angle speed which deteriorate the synchronization stability.

- Considering K_p and K_i, assuming $\omega_{pll}\neq\omega_g$, the swing equation and initial angle speed are shown as,

$$\underbrace{\omega_g L_g I_{\max}}_{P_T} - \underbrace{U_{gcp}\sin\delta}_{P_E} = \underbrace{\frac{1\text{-}K_p L_g I_{\max}}{K_i}}_{J}\delta'' + \underbrace{\left(\frac{K_p U_{gcp}\cos\delta}{K_i}\text{-}L_g I_{\max}\right)}_{D}\delta' \tag{8}$$

$$\delta_i' = \frac{K_p \omega_g L_g I_{\max}}{1 - K_p L_g I_{\max}} \tag{9}$$

Note that the reactance under synchronous reference frame is not a constant in transient process, i.e. $\omega_{pll}L_g=(\omega_g+\delta')L_g$. This phenomenon is caused by the dynamic of PLL output, and this influence is more obvious with larger grid inductance L_g. When the GFC decreases the active current after extremely severe grid voltage sags, this phenomenon can be ignored [9].

It can be found that there is a negative damping $-L_g I_{\max}$, resulting in worse synchronization stability. The initial angle speed is faster when $0<K_p L_g I_{\max}<1$, then increases the risk of LOS. Increasing K_p can increase the damping coefficient, but it will also enhance the initial angle speed to deteriorate the synchronization stability.

IV. Proposed Synchronization Stability Enhancement Scheme and Simulation Results

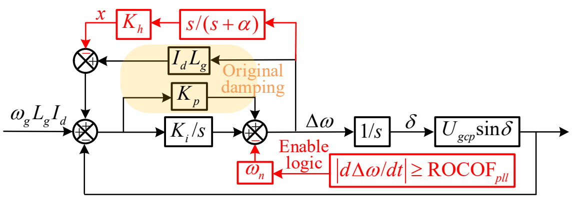

Fig. 4. Quasi-static large-signal model of the grid-following converter and proposed synchronization stability enhancement scheme.

Fig. 4 depicts the quasi-static large-signal model of the GFC. And the basic idea is to add a positive damping and a reverse angular frequency during transient process. The additional damping parameter K_h is set as $2I_dL_g$=1.7933 in this letter. The added high-pass filter is to avoid the steady-state offset in $\Delta\omega$, where the cut-off frequency is 5 Hz. When the rate of change of frequency (ROCOF) exceeds the threshold value, a reverse angular frequency $\omega_n=2\pi\cdot5$ rad/s is employed to further enhance the synchronization stability. Fig. 5, Fig. 6 and Fig. 7 validate the effectiveness of proposed scheme from *Case 1* to *Case 3*, where U_{gcp}=690 V, $I_{\max}$=1775 A, K_p=0.2, K_i=10. The blue lines denote the proposed control is disabled, and the red lines denote the proposed control is enabled.

- *Case 1:* Active current startups: I_d increases from 0 to $I_{\max}$, L_g=0.86 mH.

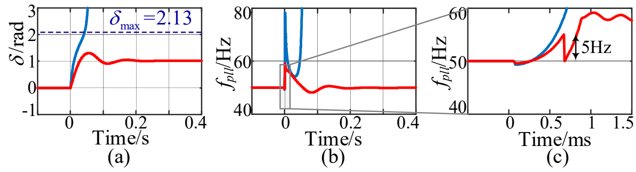

Fig. 5. Angle and frequency response for Case 1.

- *Case 2:* Line tripping fault: L_g increases from 0.1 mH to 0.89 mH.

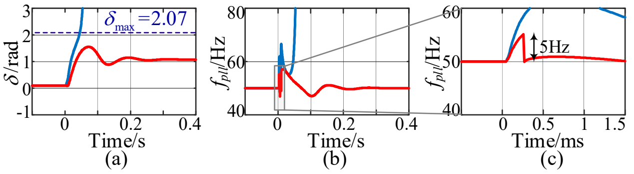

Fig. 6. Angle and frequency response for Case 2.

- *Case 3:* Grid voltage sags: U_{gcp} decreases from 690 V to 373V, L_g=0.51 mH.

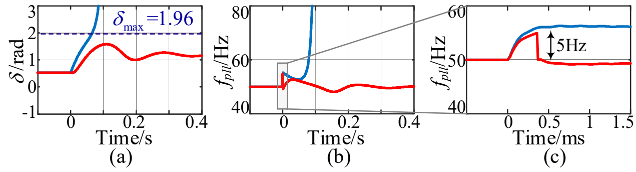

Fig. 7. Angle and frequency response for Case 3.

It is noticed that when enabling the proposed control, δ will not exceed $\delta_{\max}$, and f_{pll} will recover to 50 Hz eventually. Fig. 5 (c), Fig. 6 (c) and Fig. 7 (c) depict the enlarged view of frequency response. Note that f_{pll} is still 50 Hz in the initial stage due to the constraints of current dynamic, but it will rise to the calculated initial value after 0.5 ms. It is easy to notice that there is a reverse 5 Hz offset after the fault occurs, which can decrease the initial angle speed. And the slower rising speed of f_{pll} is caused by the positive damping. Compared with the frozen PLL, the proposed control has more accurate phase-tracking ability during grid fault. Compared with the first-order PLL, the logic transitions of proposed control are simpler, since it only need to judge when the reverse angular frequency should be enabled.

According to Fig. 4, the model considering the additional damping can be elaborated in (10). Fig. 8 depicts the synchronization stable range with parameter deviations, where the blue area indicates that the system is synchronization stable. A constant ω_n is subtracted in δ_i' to simulate the additional reverse angular frequency. It can be noticed that the α has an upper limit as 16.2 rad/s when ω_n=0, indicating the system will lose synchronization stability with high cut-off frequency of high-pass filter. When α is $2\pi\cdot2$ rad/s, K_h is necessary to set between 2.2 and 18.2. However, a too small cut-off frequency will affect the dynamic response at fundamental frequency.

The appropriate reverse angular frequency can increase the synchronization stable range and increase the upper limit of α, i.e., $\omega_n = 2\pi\cdot 2$ rad/s and $\omega_n = 2\pi\cdot 5$ rad/s. However, adding a too large reverse angular frequency may cause the reversed direction of the initial angle speed, which deteriorates the synchronization stability, i.e., $\omega_n = 2\pi\cdot 10$ rad/s.

$$\begin{cases} \left(\delta'\right)' = \dfrac{K_p(\alpha x - U_{gcp}\cos\delta\delta') + K_i\left((\omega_g + \delta')L_g I_d - U_{gcp}\sin\delta - x\right)}{1 - K_p L_g I_d + K_p K_h} \\ \left(x\right)' = K_h\left[\dfrac{K_p(\alpha x - U_{gcp}\cos\delta\delta') + K_i\left((\omega_g + \delta')L_g I_d - U_{gcp}\sin\delta - x\right)}{1 - K_p L_g I_d + K_p K_h}\right] - \alpha x \end{cases} \tag{10}$$

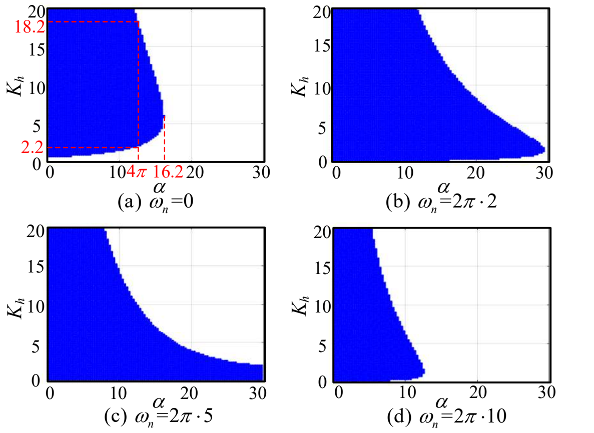

Fig. 8. Synchronization stable range with parameter deviations for Case 3.

V. Conclusions

This letter compares the swing equation between SG and GFC, then explains that when GFC encounters some grid faults such as line tripping and voltage sags, the larger positive damping and smaller absolute value of initial angle speed can enhance the synchronization stability and avoid LOS. A synchronization stability enhancement scheme is presented to increase the positive damping and decrease the initial angle speed, which has the simple logic transitions.

References

[1] K. Liao, B. Pang, J. Yang and Z. He, "Compensation strategy of wideband voltage harmonics for doubly-fed induction generator," *IEEE Trans. Energy Convers.*, vol. 38, no. 1, pp. 674-684, Mar. 2023.

[2] Y. Liu et al., "Transient stability enhancement control strategy based on improved PLL for grid connected VSC during severe grid fault," *IEEE Trans. Energy Convers.*, vol. 36, no. 1, pp. 218-229, Mar. 2021.

[3] M. G. Taul, X. Wang, P. Davari, and F. Blaabjerg, "Robust fault ride through of converter-based generation during severe faults with phase jumps," *IEEE Trans. Ind. Appl.*, vol. 56, no. 570–583, Jan. 2020.

[4] H. Wu and X. Wang, "Transient stability impact of the phase-locked loop on grid-connected voltage source converters," in *Proc. Int. Power Electron. Conf.*, 2018, pp. 2673–2680.

[5] H. Wu and X. Wang, "Design-oriented transient stability analysis of PLL-synchronized voltage-source converters," *IEEE Trans. Power Electron.*, vol. 35, no. 4, pp. 3573–3589, Apr. 2020.

[6] B. Hu, H. Nian, M. Li, Y. Liao, J. Yang and H. Tong, "Impedance characteristic analysis and stability improvement method for DFIG system within PLL bandwidth based on different reference frames," *IEEE Trans. Ind. Electron.*, vol. 70, no. 1, pp. 532-543, Jan. 2023.

[7] A. A. Nazib, D. G. Holmes, and B. P. McGrath, "Enhanced transient performance of a self-synchronising inverter during start up and severe grid fault conditions," in *Proc. IEEE 9th Int. Power Electron. Motion Control Conf. (IPEMC-ECCE Asia)*, Nov. 2020, pp. 1167–1174.

[8] Y. Ma, D. Zhu, Z. Zhang, X. Zou, J. Hu and Y. Kang, "Modeling and transient stability analysis for Type-3 wind turbines using singular perturbation and lyapunov methods," *IEEE Trans. Ind. Electron.*, vol. 70, no. 8, pp. 8075-8086, Aug. 2023.

[9] X. He, H. Geng, R. Li, and B. C. Pal, "Transient stability analysis and enhancement of renewable energy conversion system during LVRT," *IEEE Trans. Sustain. Energy.*, vol. 11, no. 3, pp. 1612–1623, Jul. 2020.